SUPPORTING INFORMATION

Reactivity of Rare-Earth Oxides in Anhydrous Imidazolium Acetate Ionic Liquid

Sameera Shah, Tobias Pietsch, Maria Annette Herz, Franziska Jach, Michael Ruck

Contents

Table S1. Results of reactions of 1 mmol La_2O_3 with 10 mmol of various imidazolium or phosphonium based ILs. In all cases, a reaction temperature of 175 °C was applied for 48 h.

ILs	Observation	Solid product
$[P_{66614}][DCA]$	Dark brown liquid with unreacted solids	La_2O_3
$[P_{66614}][Cl]$	White suspension	La_2O_3
$[P_{66614}][Nf_2T]$	White suspension	La_2O_3
$[P_{66614}][OAc]$	White suspension	La_2O_3
[BMIm][OAc]	Light brown liquid	___
[BMIm][Cl]	White suspension	La_2O_3
$[BMIm][Nf_2T]$	White suspension	La_2O_3

Table S2. Reaction parameters of various RE_2O_3 used in this work. In all cases, the reaction temperature was 175 °C.

RE_2O_3	[BMIm][OAc] : [BMIm][Cl]	Duration [h]	Yield [%]	Observation	Solid product or residual
La_2O_3	10 : 0 or 10 : 1	16	85	transparent yellow liquid	$[BMIm]_2[La_2(OAc)_8]$
Ce_2O_3	10 : 0 or 10 : 1	16	79	transparent yellow liquid	$[BMIm]_2[Ce_2(OAc)_8]$
Pr_2O_3	10 : 0 or 10 : 1	16	84	transparent yellow liquid	$[BMIm]_2[Pr_2(OAc)_8]$
Nd_2O_3	10 : 0 or 10 : 1	16	84	transparent yellow liquid	$[BMIm]_2[Nd_2(OAc)_8]$
Sm_2O_3	10 : 0 or 10 : 1	16	84	transparent yellow liquid	$[BMIm]_2[Sm_2(OAc)_8]$
Eu_2O_3	10 : 0 or 10 : 1	16	83	transparent yellow liquid	$[BMIm]_2[Eu_2(OAc)_8]$
Gd_2O_3	10: 5	48	70	transparent yellow liquid	$[BMIm]_2[Gd_2(OAc)_8]$
Tb_2O_3	10: 5	48	70	transparent yellow liquid	$[BMIm]_2[Tb_2(OAc)_8]$
Dy_2O_3	10: 5	48	70	transparent yellow liquid	$[BMIm]_2[Dy_2(OAc)_8]$
Ho_2O_3	10: 5	48	25	unreacted solid in dark brown liquid	$[BMIm]_2[Ho_2(OAc)_8]$ and Ho_2O_3
Er_2O_3	10: 5	48	96 % of solid	unreacted solid in dark brown liquid	Er_2O_3
Lu_2O_3	10: 5	48	99 % of solid	unreacted solid in dark brown liquid	Lu_2O_3
Sc_2O_3	10: 5	48	99 % of solid	unreacted solid in dark brown liquid	Sc_2O_3
Y_2O_3	10: 5	48	99 % of solid	unreacted solid in dark brown liquid	Y_2O_3
La_2O_3 + Sc_2O_3	10: 5	16	99 % of solid	unreacted solid in dark brown liquid	Sc_2O_3
La_2O_3 + Lu_2O_3	10: 5	16	99 % of solid	unreacted solid in dark brown liquid	Lu_2O_3
Eu_2O_3 + Y_2O_3	10: 5	16	99 % of solid	unreacted solid in dark brown liquid	Y_2O_3
Eu_2O_3 + CeO2	10: 5	16	99 % of solid	unreacted solid in dark brown liquid	CeO_2

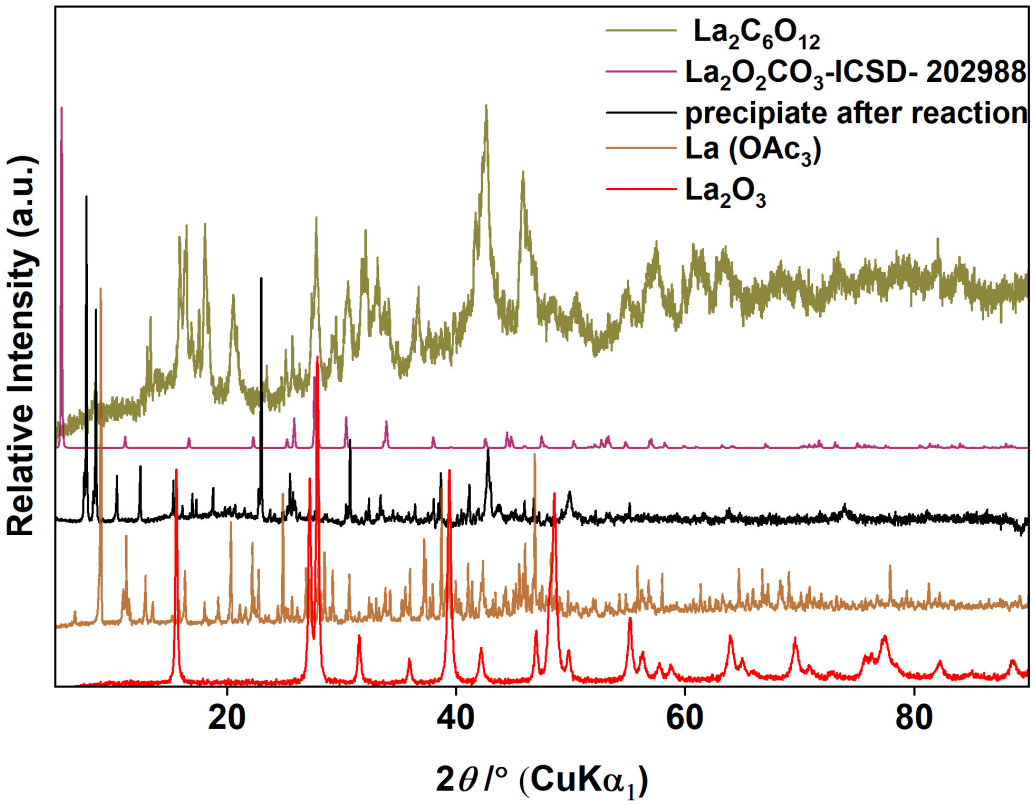

Figure S1. PXRD pattern of the white microcrystalline precipitate that formed by the reaction of La_2O_3 with [BDMIm][OAc] and acetic acid at room temperature together with the patterns of some reference compounds.

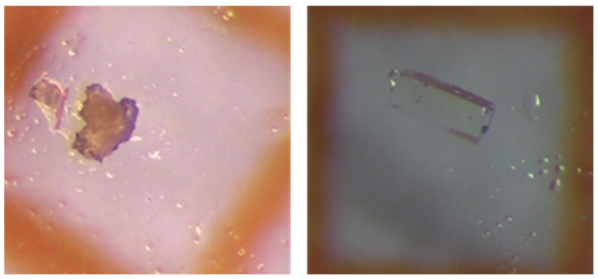

Figure S2. Crystals of $[BMIm]_2[La_2(OAc)_8]$ formed in the absence (left) or presence of chloride (right).

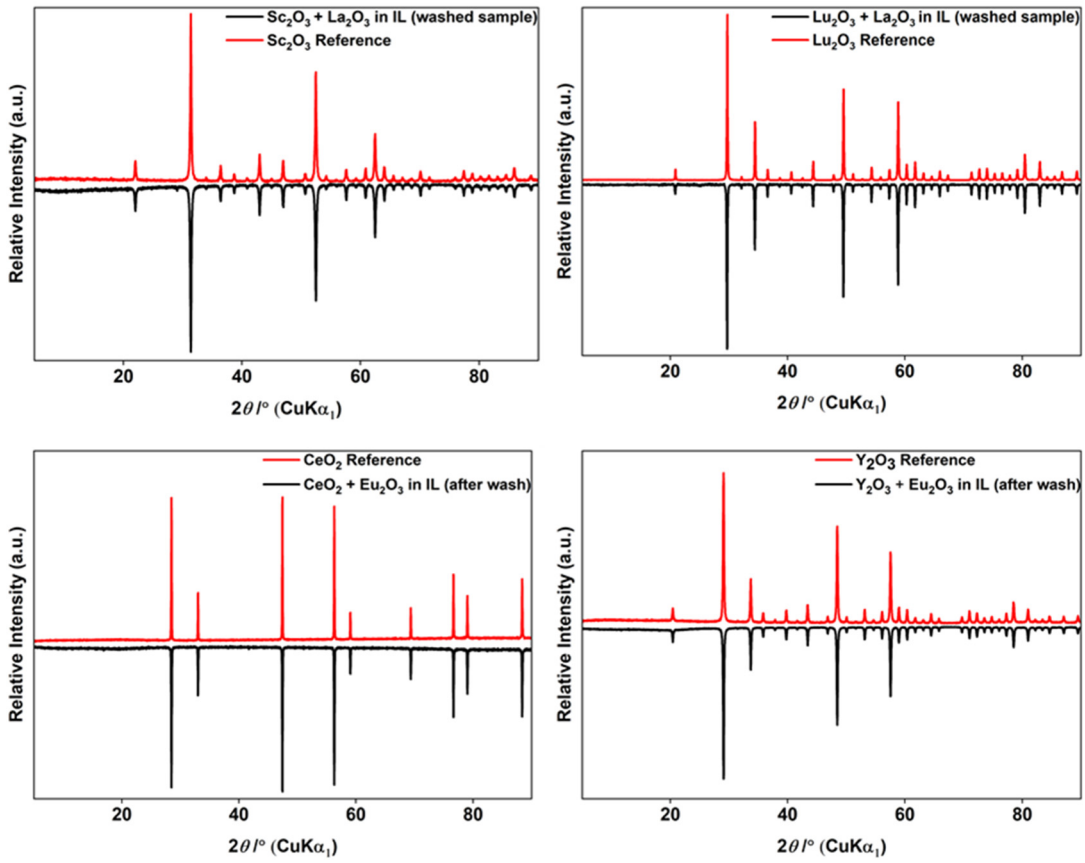

Figure S3. PXRD diffractograms of the solid residuals after selective solution of one component from the mixtures La_2O_3/Sc_2O_3, La_2O_3/Lu_2O_3, Eu_2O_3/Y_2O_3, and Eu_2O_3/CeO_2.

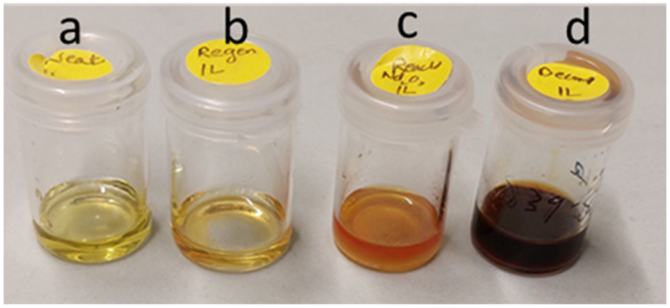

Figure S4. Pure [BMIm][OAc] (a), regenerated IL (b), La_2O_3 dissolved in the IL (c), and decomposed IL (d).

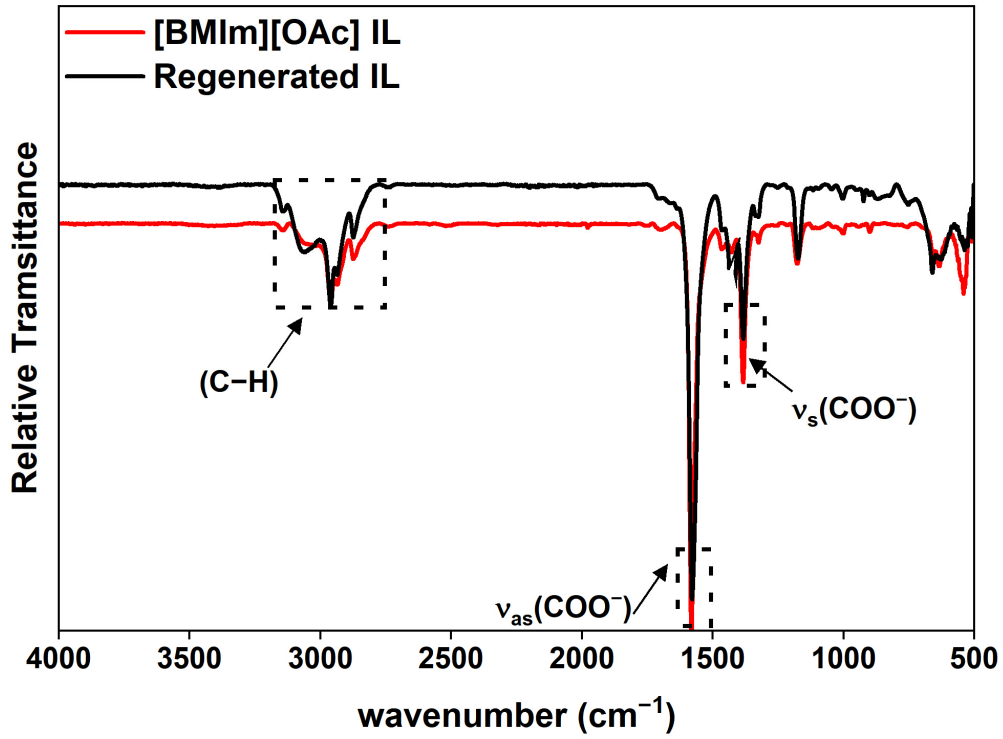

Figure S5. FTIR spectra of neat and regenerated [BMIm][OAc].

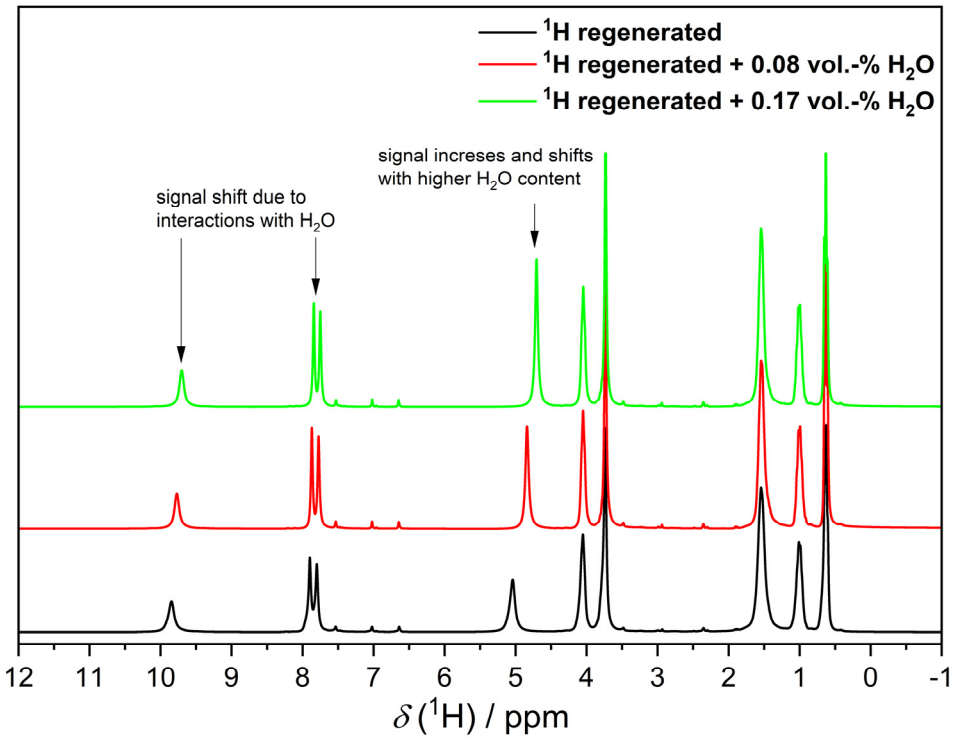

Figure S6. ^{1}H NMR spectra of regenerated [BMIm][OAc] with different water content.

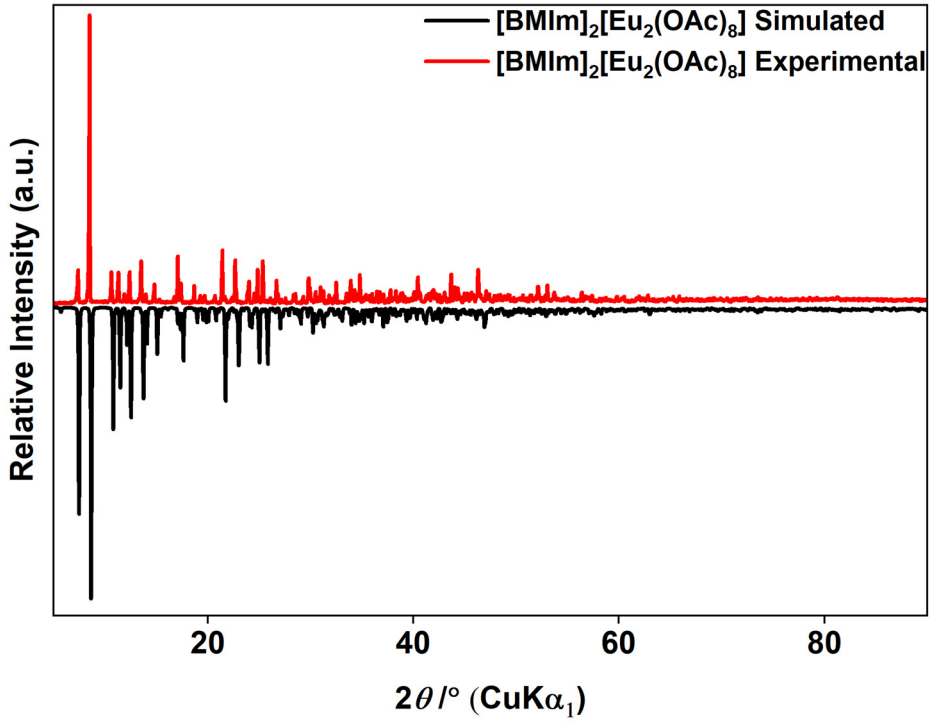

Figure S7. Simulated (based on crystal structure) and measured powder X-ray diffractogram of $[BMIm]_2[Eu_2(OAC)_8]$.

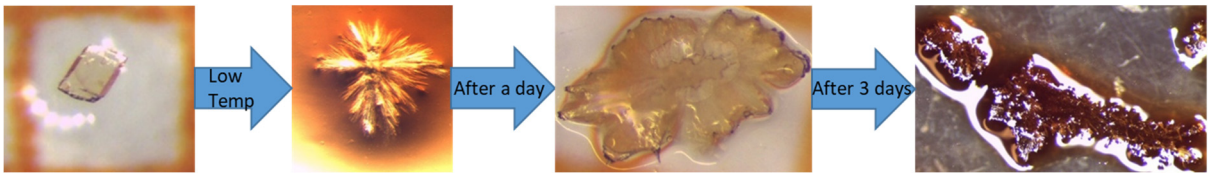

Figure S8. On cooling, the crystals of $[BMIm]_2[Dy_2(OAc)_8]$ changed to needle like morphology, after one day to snow-like flakes, then on further cooling dendrites formed that decomposed after few days. Due to very weak intensity, we could not measure single-crystal diffraction data, however, the PXRD and FT-IR analysis showed a structural change.

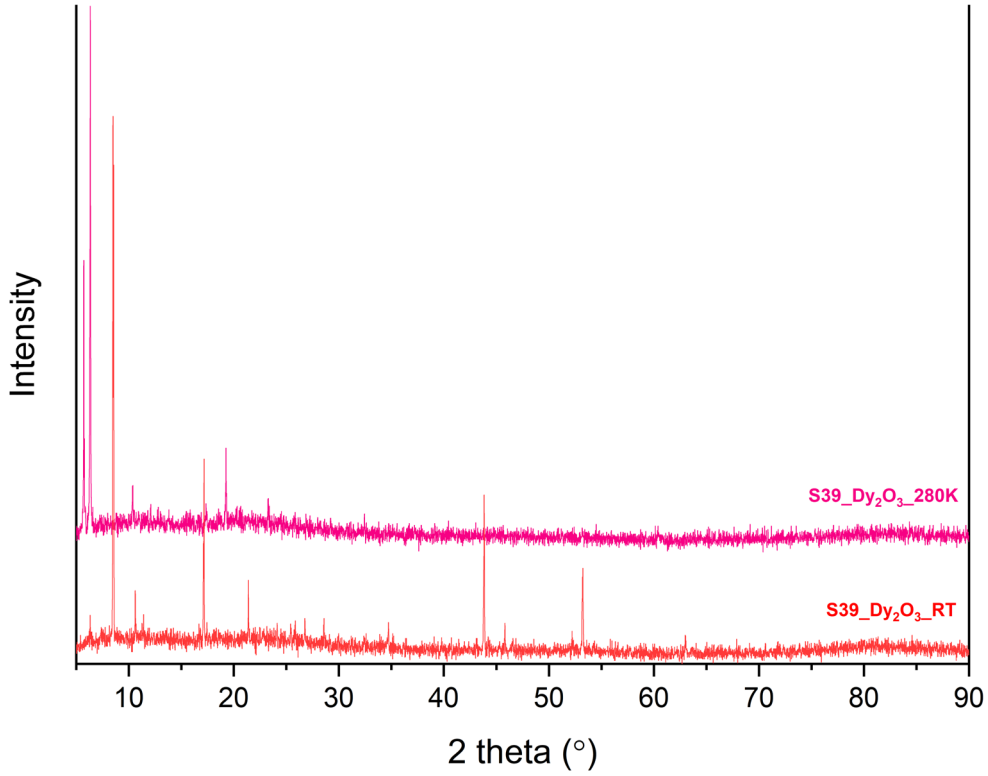

Figure S9. PXRD diffractogram measured at 100 K of $[BMIm]_2[Dy_2(OAc)_8]$ crystals grown at room temperature or at 5 °C.

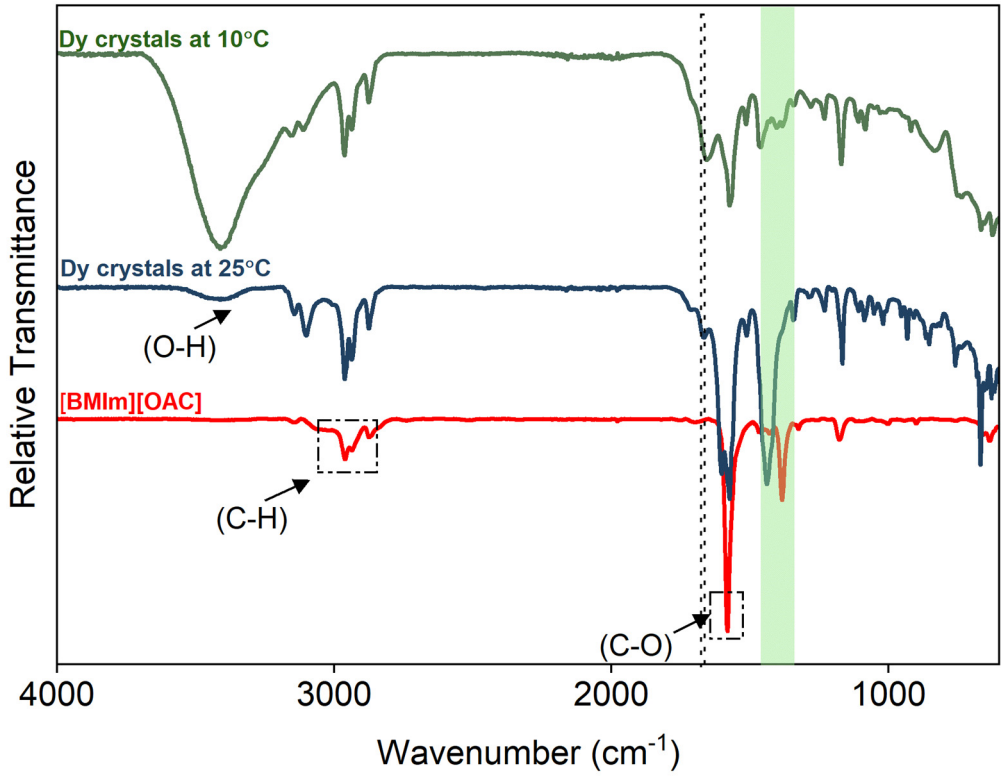

Figure S10. FTIR spectra of the IL and $[BMIm]_2[Dy_2(OAc)_8]$ crystals grown at room temperature or at 5 °C.

Table S3. Crystallographic data for $[BMIm]_2[RE_2(OAc)_8]$ salts at 100(2) K.

RE	La	Pr	Nd	Sm
Crystal system	triclinic	triclinic	triclinic	triclinic
Space group	$P\bar{1}$ (no. 2)	$P\bar{1}$ (no. 2)	$P\bar{1}$ (no. 2)	$P\bar{1}$ (no. 2)
a / Å	12.1364(3)	12.0863(4)	8.410(1)	8.4141(3)
b / Å	13.7492(4)	13.6472(4)	15.714(2)	15.6356(5)
c / Å	14.4262(4)	14.4723(4)	16.071(2)	16.0023(5)
α / °	110.294(1)	110.460(2)	98.253(4)	98.088(2)
β / °	102.682(1)	102.248(2)	103.809(4)	103.858(2)
γ / °	104.303(1)	104.517(2)	90.271(4)	90.347(2)
V / Å^3	2060.8(1)	2043.5(1)	2039.4(4)	2021.9(1)
Z	2	2	2	2
$\rho_{calc.}$ / (g cm^{-3})	1.658	1.678	1.692	1.727
μ(Mo-K$_\alpha$) / mm^{-1}	2.12	2.43	2.59	2.95
Crystal size / μm^3	31 × 60 × 70	39 × 65 × 65	25 × 50 × 58	74 × 89 × 104
$2\theta_{max}$ / °	72.8	78.3	64.5	78.6
Index range	–20 ≤ *h* ≤ 19 –22 ≤ *k* ≤ 22 –24 ≤ *l* ≤ 23	–21 ≤ *h* ≤ 19 –22 ≤ *k* ≤ 24 –25 ≤ *l* ≤ 23	–12 ≤ *h* ≤ 12 –23 ≤ *k* ≤ 23 –23 ≤ *l* ≤ 23	–14 ≤ *h* ≤ 14 –27 ≤ *k* ≤ 27 –28 ≤ *l* ≤ 28
Reflections measured, unique, $F_o > 4\ F_o$	168374, 19752, 15880	191624, 23834, 17119	86255, 13673, 10410	256225, 23661, 19897
R_{int}, R_σ	0.039, 0.029	0.043, 0.037	0.054, 0.043	0.053, 0.031
Parameters, restraints	564, 132	564, 132	499, 0	499, 0
$R_1[F_o > 4\sigma(F_o)]$, wR_2(all), *GooF*	0.027, 0.057, 1.32	0.037, 0.046, 1.86	0.029, 0.043, 1.26	0.025, 0.037, 1.44
Residual electron density / (e · 10^{-6} pm^{-3})	–1.32 to 2.87 close to La	–2.71 to 2.52 close to Pr	–1.06 to 1.08 close to Nd	–1.32 to 1.19 close to Sm

Table S3 (continued)

RE	Eu	Tb	Ho
Crystal system	triclinic	triclinic	triclinic
Space group	$P\bar{1}$ (no. 2)	$P\bar{1}$ (no. 2)	$P\bar{1}$ (no. 2)
a / Å b / Å c / Å α / ° β / ° γ / ° V / Å^3	8.4242(3) 15.6486(6) 16.0129(7) 98.039(1) 103.845(1) 90.314(1) 2027.8(1)	8.4144(4) 15.5531(8) 15.9555(8) 97.829(3) 103.998(3) 90.379(3) 2005.5(2)	8.4180(3) 15.5315(5) 15.9429(6) 97.785(2) 103.976(2) 90.383(2) 2002.4(1)
Z	2	2	2
$\rho_{calc.}$ / (g cm^{-3})	1.727	1.770	1.792
μ(Mo-K$_\alpha$) / mm^{-1}	3.14	3.57	4.00
Crystal size / µm^3	36 × 42 × 51	37 × 43 × 56	19 × 25 × 38
$2\theta_{max}$ / °	69.0	73.1	69.8
Index range	–13 ≤ h ≤ 13 –24 ≤ k ≤ 24 –25 ≤ l ≤ 25	–14 ≤ h ≤ 14 –25 ≤ k ≤ 25 –26 ≤ l ≤ 26	–13 ≤ h ≤ 13 –24 ≤ k ≤ 24 –25 ≤ l ≤ 25
Reflections measured, unique, $F_o > 4\ F_o$	117435, 17220, 13545	178745, 19404, 13740	154211, 16615, 12526
R_{int}, R_σ	0.050, 0.035	0.104, 0.070	0.057, 0.041
Parameters, restraints	499, 0	499, 0	499, 0
$R_1[F_o > 4\sigma(F_o)]$, wR_2(all), *GooF*	0.026, 0.034, 1.31	0.041, 0.070, 1.19	0.029, 0.034, 1.37
Residual electron density / (e · 10^{-6} pm^{-3})	–0.99 to 1.23 close to Eu	–3.28 to 1.83 close to Tb	–1.20 to 1.78 close to Ho

Table S4. Metal-metal and metal-oxygen bond distances of all complexes studied in this work.

Complex salt	*RE*-*RE* distance (Å)	*RE*-O distance (Å)
[BMIm]$_2$[La$_2$(OAc)$_8$]	4.061(1)	2.454(0)–2.639(1)
[BMIm]$_2$[Pr$_2$(OAc)$_8$]	4.000(1)	2.432(1)–2.629(1)
[BMIm]$_2$[Nd$_2$(OAc)$_8$]	3.990(2)	2.420(2)–2.592(2)
[BMIm]$_2$[Sm$_2$(OAc)$_8$]	3.911(1)	2.366(1)–2.564(1)
[BMIm]$_2$[Eu$_2$(OAc)$_8$]	3.905(1)	2.357(1)–2.532(1)
[BMIm]$_2$[Tb$_2$(OAc)$_8$]	3.865(2)	2.323(1)–2.537(1)
[BMIm]$_2$[Ho$_2$(OAc)$_8$]	3.845(1)	2.302(1)–2.517(1)

Table S5. Selected interatomic distances (/Å) in the Eu and La compounds, which belong to different structure types.

Atom pair	*d* [Å]	Atom pair	*d* [Å]	*d* [Å]	*d* [Å]
Eu2···Eu2	3.938(1)	**La1···La2**	4.061(1)	**La2–O11**	2.630(1)
Eu1···Eu1	3.905(1)	**La1–O1**	2.573(1)	**La1–O12**	2.479(0)
		La1–O2	2.566(1)	**La1–O13**	2.461(1)
Eu1–O1	2.498(1)	**La1–O3**	2.558(1)	**La2–O14**	2.474(1)
Eu1–O2	2.482(1)	**La1–O4**	2.573(1)	**La2–O15**	2.486(1)
Eu1–O3	2.498(1)	**La2–O5**	2.592(1)	**La1–O16**	2.485(1)
Eu1–O4	2.462(1)	**La2–O6**	2.566(1)		
Eu1–O5	2.392(1)	**La2–O7**	2.581(1)		
Eu1–O6	2.383(1)	**La2–O8**	2.555(1)		
Eu1–O7	2.357(1)	**La1–O9**	2.639(1)		
Eu1–O8	2.532(1)	**La2–O10**	2.454(1)		

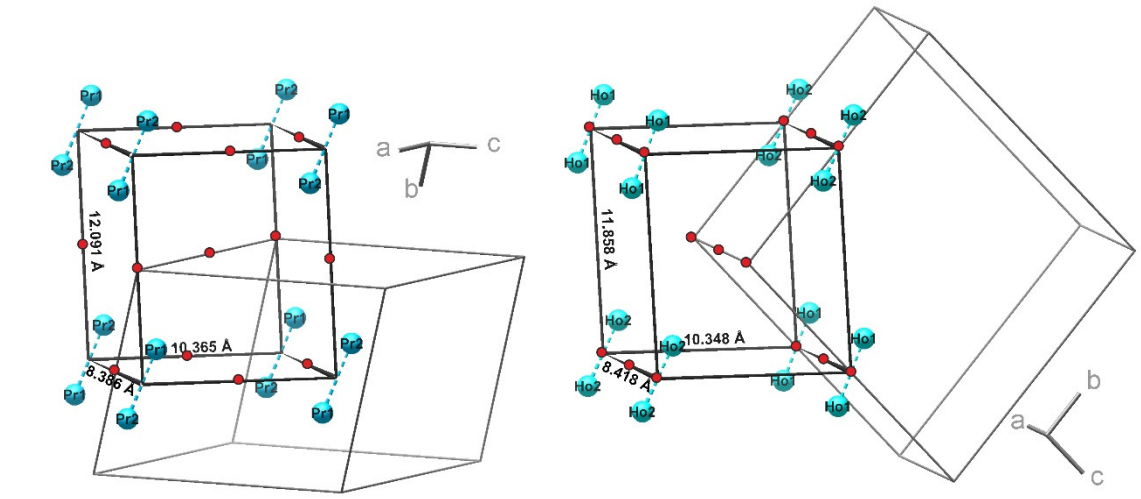

Figure S11. Analogous sections of the structures of $[BMIm]_2[Pr_2(OAc)_8]$ (left) and $[BMIm]_2[Ho_2(OAc)_8]$ (right), reduced to their *RE* cations. The analogous subcells of the two structure types emphasize the different positions of the RE^{3+} cations relative to the centers of inversion (indicated as red dots). Translational pseudosymmetry is observed (pseudo-B-centering left, pseudo-A-centering right). Angles in the specified subcells for the Pr/Ho compound (dark axes, sorted according to increasing length): α = 91.2°/91.2°, β = 98.1°/101.6 °, γ = 99.4°/99.5°.

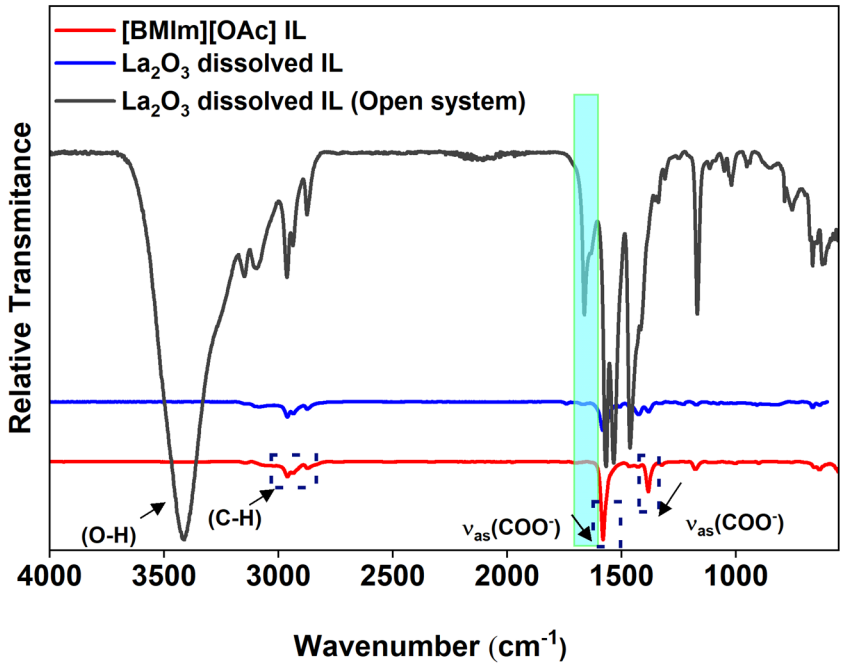

Figure S12. FTIR spectra of neat [BMIm][OAc], a fresh solution of La_2O_3 in the IL, and a solution with decomposed IL.

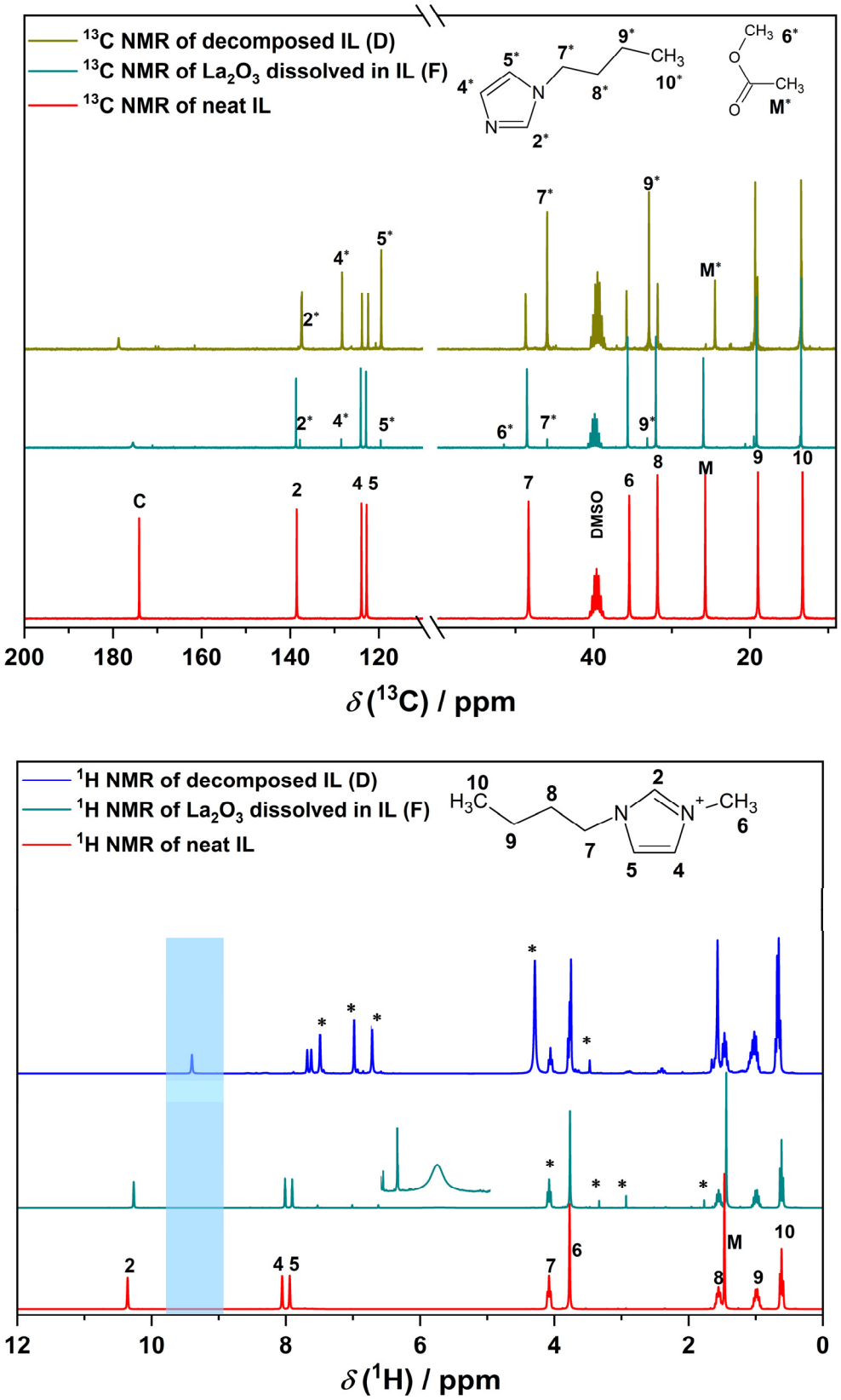

Figure S13. ^{13}C (top) and ^{1}H NMR (bottom) spectra of neat [BMIm][OAc], of a freshly prepared solution of La_2O_3 in the IL, and of a solution with largely decomposed IL.

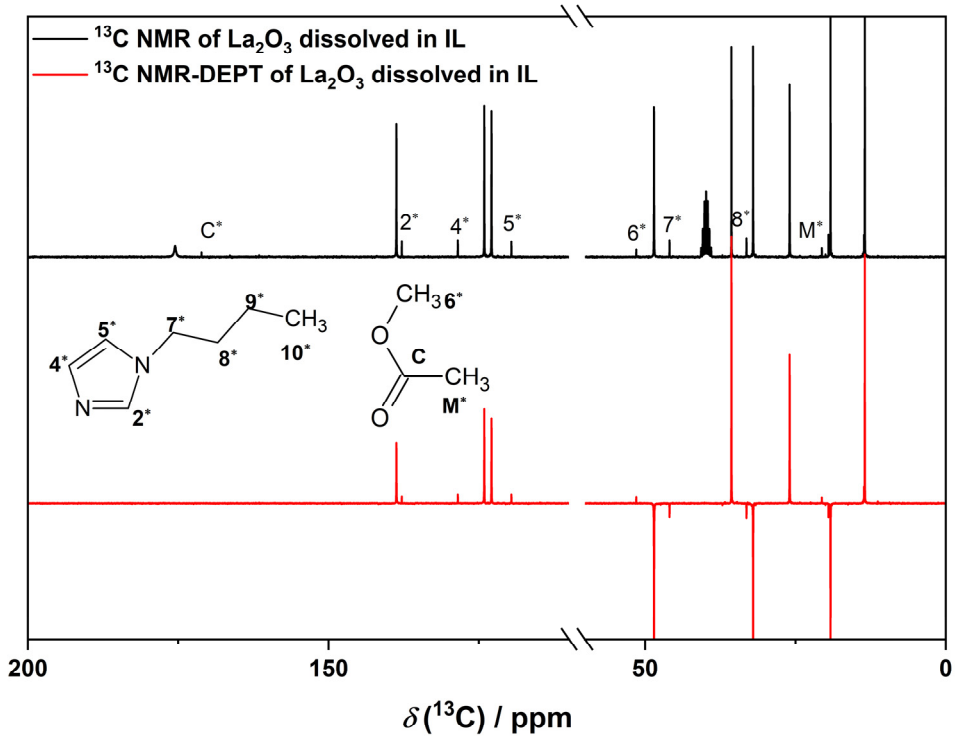

Figure S14. ^{13}C NMR spectrum and DEPT 135 ^{13}C NMR spectrum of a freshly prepared La_2O_3 solution in [BMIm][OAc].

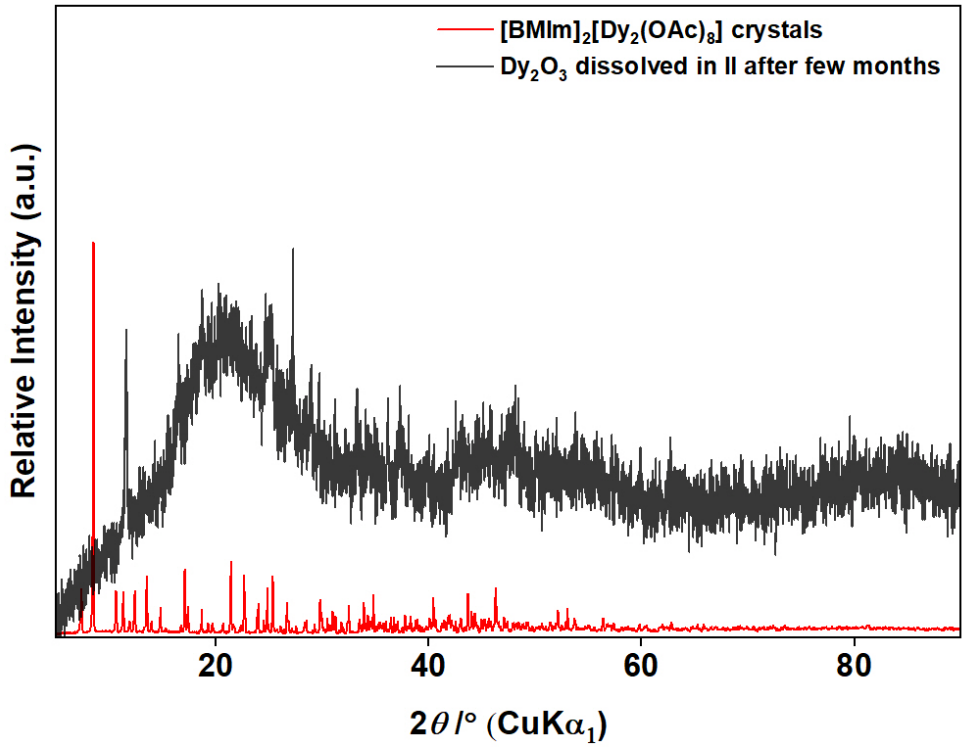

Figure S15. Degradation of $[BMIm]_2[Dy_2(OAc)_8]$ crystals in the reaction mixture after one month in air.

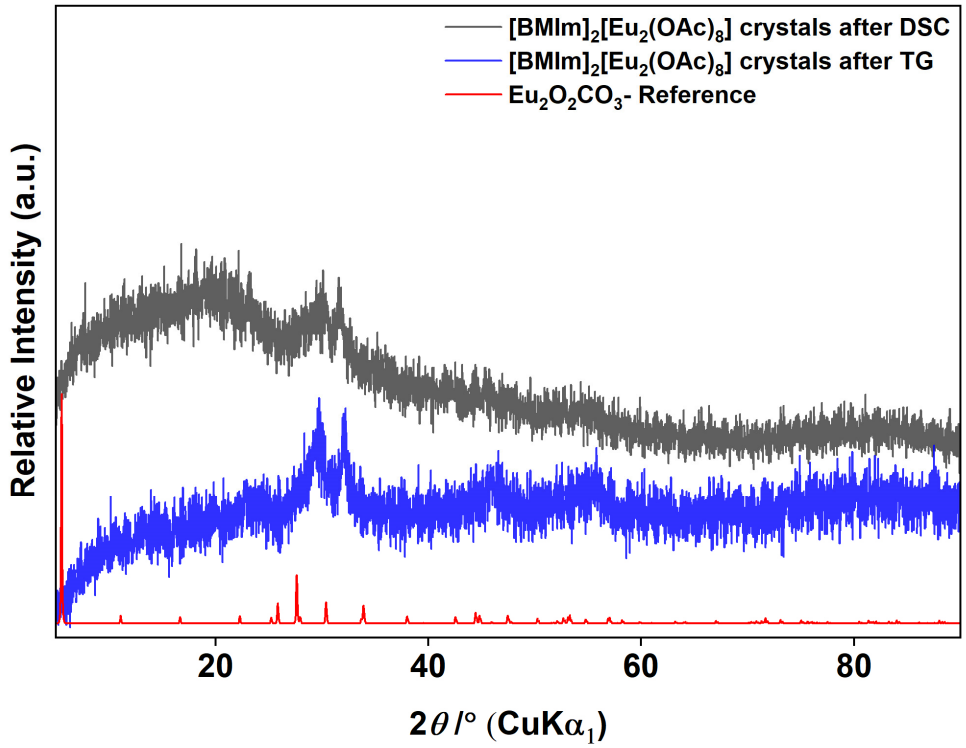

Figure S16. PXRD diffractogram of $[BMIm]_2[Eu_2(OAc)_8]$ samples after DSC or after TG under argon with a maximum temperature of 500 °C.

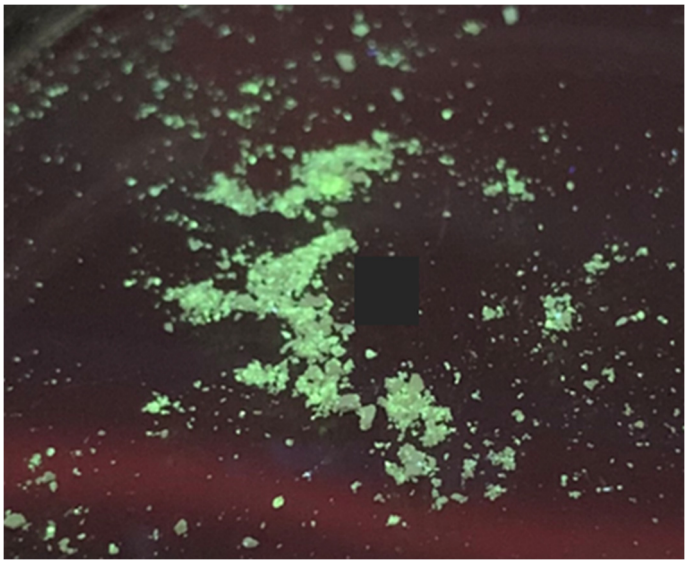

Figure S17. Luminescence of $[BMIm]_2[Tb_2(OAc)_8]$ under UV light of 312 nm.

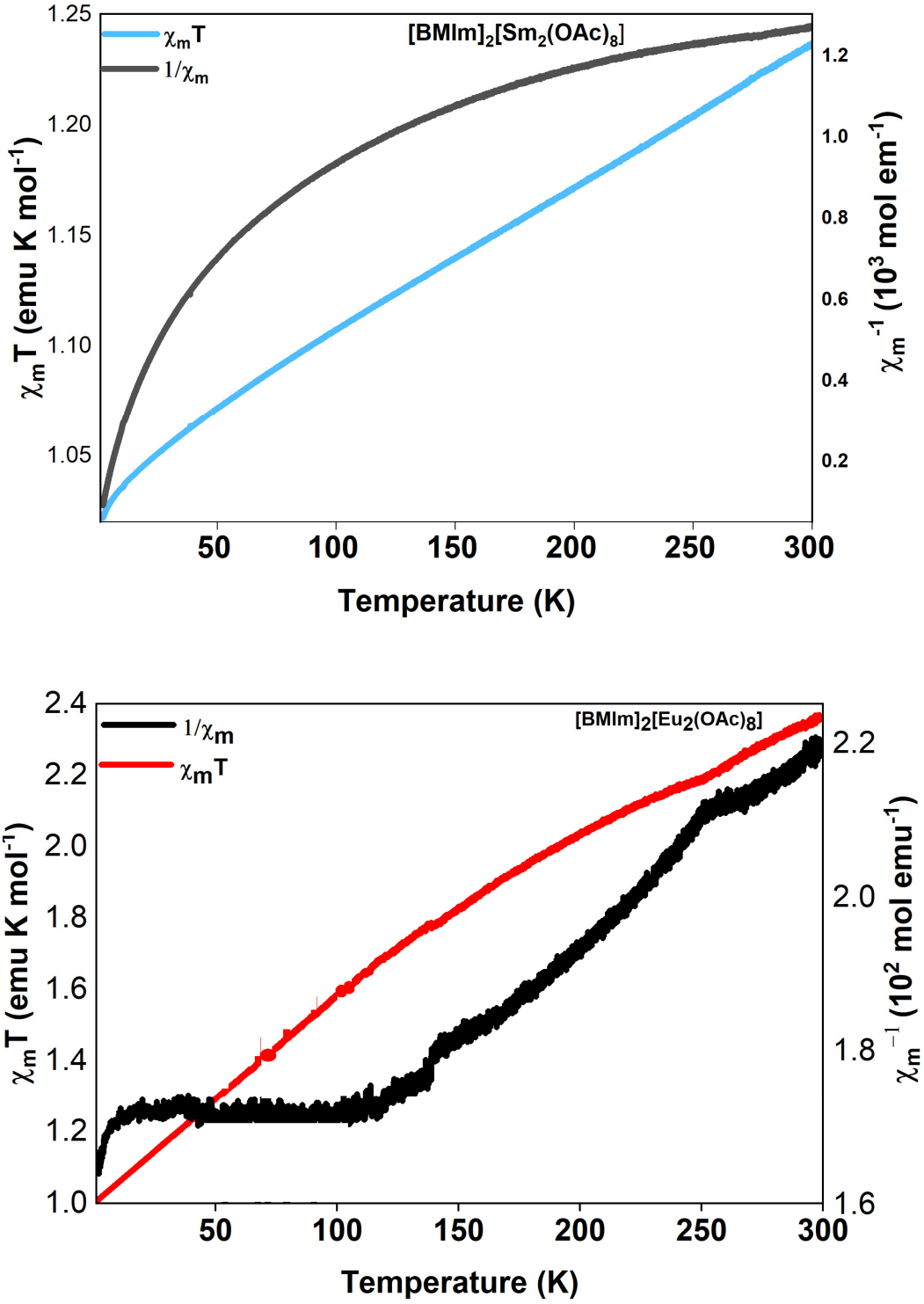

Figure S18. $\chi_m T$ and χ_m^{-1} plots for $[BMIm]_2[Sm_2(OAc)_8]$ and $[BMIm]_2[Eu_2(OAc)_8]$.

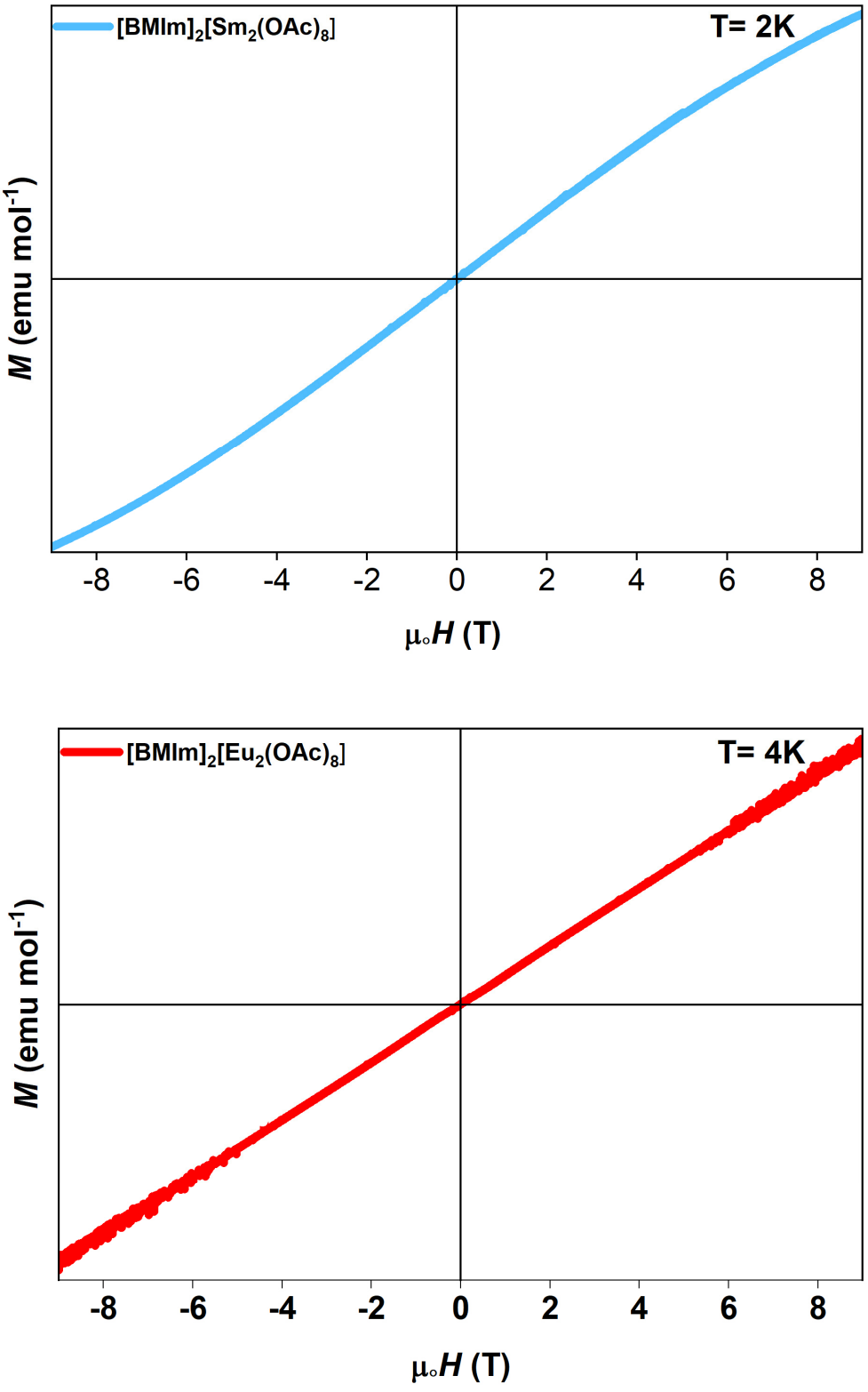

Figure S19. Magnetization (*M*) versus field (*H*) for $[BMIm]_2[Sm_2(OAc)_8]$ and $[BMIm]_2[Eu_2(OAc)_8]$.